ELSEVIER

International Journal of Mass Spectrometry 219 (2002) 115–131

International Journal of Mass Spectrometry

www.elsevier.com/locate/ijms

Effects of peptide chain length on the gas-phase proton transfer properties of doubly-protonated ions from bradykinin and its N-terminal fragment peptides

Giovanni A. Pallante[1] , Carolyn J. Cassady*

Department of Chemistry, University of Alabama, Tuscaloosa, AL 35406, USA

Received 20 July 2001; accepted 20 December 2001

Abstract

Proton transfer properties were studied for doubly-protonated ions from bradykinin and seven smaller peptides whose sequences have C-terminal residues successively removed from bradykinin. Ions were generated by electrospray ionization (ESI) and their deprotonation reactions were investigated in a Fourier transform ion cyclotron resonance mass spectrometer. Sustained off-resonance irradiation (SORI)-collision-induced dissociation (CID) was used to obtain information on sites of protonation, while molecular dynamics calculations provided information on peptide ion conformations and Coulomb energies. As the number of amino acid residues decreases the peptide ions undergo proton transfer more readily. Apparent gas-phase acidities (GA_{app}s), for the doubly-protonated ions decreased as the peptide size decreased, with values spanning the range of 225.8 ± 4.2 kcal/mol for the nonapeptide bradykinin to 196.6 ± 4.4 kcal/mol for the tripeptide $Arg^1Pro^2Pro^3$. The magnitude of the drop in GA_{app} as a residue was removed varied from 10.9 kcal/mol for removal of the highly basic Arg^9 to 0 kcal/mol for removal of Phe^8 (whose phenylalanine ring juts away from the peptide backbone and does not participate in hydrogen bonding). Hydrogen bonding in the modeled structures decreased as the peptide chain length decreased. The lowest energy structure for doubly-protonated bradykinin contained nine hydrogen bonds, while only one hydrogen bond was found for the tripeptide ions. In addition, the tripeptide ions had an extended structure, while the larger peptide ions were compact. There is no single reason that the peptide ions become more acidic (i.e., more reactive to proton transfer) as the peptide chain length is decreased. Depending upon the situation, factors that play a role in the proton transfer reactivity include intrinsic basicity of the protonation sites, intramolecular hydrogen bonding (particularly involving the protonated residue), Coulombic repulsion of charge sites, and conformational considerations such as accessibility/shielding of the protonation site. (Int J Mass Spectrom 219 (2002) 115–131)

Keywords: Bradykinin; SORI; CID; FT-ICR; Proton transfer

1. Introduction

The gas-phase proton transfer properties of peptides and their ions have been the focus of numerous studies in the past decade. Proton transfer is important to biological mass spectrometry because the ionization event often involves the addition of protons to the peptide. The locations of these added protons can affect how a peptide dissociates under MS/MS conditions and can thus impact the sequence information that is obtained [1–8].

* Corresponding author. E-mail: cassadcj@ua.edu

[1] Present address: PHARMACIA, 7265-300-305, 301 Henrietta St., Kalamazoo, MI 49007, USA.

1387-3806/02/$ – see front matter
PII S1387-3806(02)00556-0

Insight into the proton transfer properties of peptide ions can be gained from gas-phase deprotonation reactions. Using a trapping mass spectrometer, the kinetics and energetics of deprotonation can be probed by employing a series of neutral reactants of known gas-phase basicity (GB) and monitoring the reaction progress as a function of time. This allows the apparent gas-phase acidity, GA_{app} [9,10] of a multiply protonated peptide $[M + nH]^{n+}$, to be measured.

Three major factors influence gas-phase deprotonation reactivity of $[M+nH]^{n+}$: intrinsic acidity/basicity of the reactive sites, Coulomb repulsion resulting when multiple charge sites are present on the reactant ion, and peptide conformation [11–13]. These factors are interrelated and have each been the subject of several studies involving multiple-charged ions produced by electrospray ionization (ESI).

The impact of intrinsic basicity of the site being deprotonated was investigated by Carr and Cassady [14] using a series of small peptides with 11–14 amino acid residues but differing sequences. Peptides with highly basic arginine residues were more difficult to deprotonate. However, in another study involving peptides with up to 76 amino acid residues, the effects of intrinsic basicity on deprotonation were shown to diminish as the size of the peptide increased [15].

The study of small peptide deprotonation [14] also revealed that Coulombic repulsion can sometimes overrule intrinsic basicity and become the deciding factor in reactivity. More facile deprotonation was evident when ions experienced Coulombic repulsion from adjacent protonation sites. This phenomenon was further probed in our laboratory using three model dodecapeptides that were all composed of four high basicity lysine (K) residues and eight low basicity glycine (G) residues [16,17] but with varying orders of the residues. Because these peptides had identical amino acid compositions, intrinsic basicity at the atom being deprotonated was not a factor in comparing reactivities. For "fully protonated" $[M + 4H]^{4+}$, the peptide with high Coulomb energy due to four adjacent lysine residues deprotonated far more readily than two peptides that had considerably less charge repulsion. In addition, a direct manifestation of the effect of Coulomb energy on proton transfer is that the rate of deprotonation increases as the number of protons attached to a peptide or protein increases [15–20].

The third factor affecting proton transfer reactivity, ion conformation, is often closely related to Coulomb energy. As the lysine–glycine dodecapeptide work illustrates [16,17], a three-dimensional structure may be elongated to maximize the distance between charge sites (i.e., minimize Coulomb energy) or the structure may compact and charge sites may be stabilized by extensive hydrogen bonding. Conformation has also been a focus of several deprotonation studies involving disulfide-intact and -reduced peptide ions [20–23]. In these studies, amino acid sequences and thus intrinsic basicities are the same for a pair of disulfide-intact and -reduced ions. There is no general rule on how cleavage of a disulfide bond, and the resulting change in conformation and Coulomb energy, will affect proton transfer reactivity. For some compounds, intact bonds give more compact structures, greater Coulomb energies, and faster rates of deprotonation. For other compounds, the enhanced flexibility of cleaved bonds results in more compact structures and faster rates. If a structure is too compact, proton transfer rates may also be lessened because the reactant neutral may have difficulty accessing the site to be deprotonated.

In the present study, we explore the effects of peptide chain length on the proton transfer properties of doubly-charged ions generated by ESI. The compounds under study are bradykinin, a common nonapeptide that has been the subject of numerous mass spectral investigations [7,24–46], and seven smaller peptides (i.e., fragments) that have the C-terminal residue sequentially removed from the bradykinin sequence. The GA_{app} for each $[M + 2H]^{2+}$ was measured by deprotonation reactions. Molecular modeling was used to provide insight into peptide ion conformation, while collision-induced dissociation (CID) yielded information on potential protonation sites.

2. Experimental

2.1. Mass spectrometry

All experiments were performed using a Bruker (Billerica, MA, USA) BioAPEX 47e Fourier transform ion cyclotron resonance (FT-ICR) mass spectrometer with a 4.7 T superconducting magnet. Ions were produced with an external Analytica of Branford (Branford, CT, USA) ESI source and moved into the ICR cell by electrostatic focusing.

Peptide solutions, with concentrations ranging from $(4 \text{ to } 8) \times 10^{-5}$ M, were prepared in a 50:50:1 mixture by volume of methanol:water:acetic acid. The solutions were introduced into the ESI source at a flow rate of 0.75 μL/min and flowed through a grounded needle at atmospheric pressure before being electrosprayed across a 4 kV potential through a heated (200 °C) CO_2 counter-current drying gas.

The apparent gas-phase acidities (GA_{app}s) of $[M + 2H]^{2+}$, which are equivalent to the apparent gas-phase basicities (GB_{app}s) of $[M+H]^+$ [9,10] were assigned using the bracketing method. This involved isolating $[M+2H]^{2+}$ by correlated ion ejection sweeps [47] and allowing these ions to react with reference compounds of known GB. The reference compounds were present in the FT-ICR analyzer vacuum chamber at static pressures of $(4–10) \times 10^{-8}$ Torr. Pressures were measured with an ion gauge that was calibrated against an ion/molecule reaction with a known reaction rate constant ($CH_4^+ + CH_4$) and corrected for reactant gas ionization efficiency [48,49]. Deprotonation rate constants were determined by observing the pseudo-first-order decay in reactant ion intensity as a function of reaction time. Reported reaction efficiencies are the ratio of the experimental rate constant to the theoretical collision rate constant, which was obtained using Su and Chesnavich parameterized trajectory (thermal capture) calculations [50,51]. A reaction efficiency break point of 0.10 was used to assign GA_{app}s values for each $[M + 2H]^{2+}$. Recent work in our laboratory [46] has shown that this efficiency criteria gives reasonable results for bradykinin analogues.

For sustained off-resonance irradiation (SORI)-CID [52] experiments, ions were activated 500–1400 Hz above and below their resonance frequencies using a 5–10V_{pp} pulse for 50–200 ms. The collision gas was a pulse of xenon that reached a maximum pressure of 10^{-5} Torr. After ion activation, a 1 s delay allowed time for collisional dissociation and for the xenon to pump away prior to the detection event.

Bradykinin and its N-terminal fragment peptides were purchased from Sigma (St. Louis, MO, USA), Bachem Bioscience (Philadelphia, PA, USA) and Quality Controlled Biochemicals (Hopkinton, MA, USA). Reference compounds were purchased from Aldrich (St. Louis, MO, USA), Eastman Kodak Company (Rochester, NY, USA) and Fisher Scientific (Fair Lawn, NY, USA). All compounds were used without additional purification.

2.2. Molecular dynamics calculations

Molecular modeling was performed with HyperChem for SGI version 4.5 from Hypercube Inc. (Waterloo, Ontario, Canada). Using amino acid structures from the HyperChem data base, starting structures were built for $[M + 2H]^{2+}$ from each peptide under study. As needed, protons were added to the N-terminal amino groups or to basic sites on the side chains of arginine or proline residues. For proline residues, this involved adding a proton to the pyrrolidine ring's –NH group. This –NH group is part of an amide linkage that includes the carbonyl group of the neighboring residue (on the N-terminal side of the peptide). For simple amides, gas-phase protonation occurs on the carbonyl oxygen rather than the nitrogen [53]. However, if the nitrogen is involved in a ring system, its basicity is frequently increased and N-protonation may become favored over O-protonation [53]. In addition, in a modeling study of peptide protonation by ESI, Schnier et al. [54] found that proline is a preferential charge site with protonation at its "side chain."

Dynamics calculations employed the Bio+ force field, which is an implementation of the CHARMM

force field [55]. In a typical simulation, the ions were heated from 0 to 500 K in 1.0 ps, followed by dynamic simulation for 15 ps with 0.001 ps time steps, and then cooling to 300 K in 2 ps. The newly obtained low energy structure was geometry optimized and used as the starting point for another simulation. Twenty-five simulations were run for each structure. During each 15 ps simulation, hundreds of snapshot files were also saved and reviewed to determine if a significant lower energy structure might have been "passed over" during the simulation. That is, although only 25 structures for each peptide were used to obtain Coulomb energy data, many more where actually acquired.

Potential energy values were obtained directly from the HyperChem program. Coulomb or electrostatic energy, ϕ, was obtained from the modeled structures using Eq. (1)

$$\text{Coulomb energy} = \phi = \sum_{ij} \frac{z_i z_j e^2}{4\pi\epsilon_0\epsilon_r r_{ij}} \quad (1)$$

where z_i and z_j are the nominal values of the interacting charges, e the charge on an electron, r_{ij} the distance between two charged atoms in the model structures, ϵ_r the dielectric constant, and ϵ_0 is a constant known as the vacuum permittivity. A value of 1.0 was used for the dielectric constant, ϵ_r; recent studies [56,57] have suggested that this value is appropriate for small multiply charged ions in the gas-phase.

3. Results and discussion

The $[M + 2H]^{2+}$ ions were isolated and deprotonated to $[M + H]^+$ using reference compounds with GBs ranging from 182.2 to 237.3 kcal/mol. Table 1 contains the measured reaction efficiencies for the reactions of $[M + nH]^{n+}$ from the peptides (M) studied with selected reference compounds (B) of known GB. The reaction monitored was

$$[M + nH]^{n+} + B \rightarrow [M + (n-1)H]^{(n-1)+} + BH^+ \quad (2)$$

The Gibbs free energy, ΔG, for the deprotonation of $[M + nH]^{n+}$, as shown in Eq. (3)

$$[M + nH]^{n+} \rightarrow [M + (n-1)H]^{(n-1)+} + H^+ \quad (3)$$

is equal to the gas-phase acidity

$$GA([M + nH]^{n+}) = \Delta G \quad (4)$$

Due to the reverse activation barrier (RAB) present in reaction 2, what is actually determined experimentally is the GA_{app}, as seen in Eq. (5) [9,15,58,59]

$$GA_{app}([M + nH]^{n+}) = GA([M + nH]^{n+}) + RAB \quad (5)$$

The GA_{app} of the reactant $[M + nH]^{n+}$ also corresponds to the apparent gas-phase basicity, GB_{app}, of the product $[M + (n-1)H]^{(n-1)+}$. The term "apparent gas-phase acidity" was first introduced by Bohme and coworkers [9,10]; it is the quantity that can be directly measured from deprotonation reactions and indicates the reactivity of $[M + nH]^{n+}$. (In contrast, GB_{app} is not directly measurable because adding a proton to an already protonated ion is barrier-inhibited and will not occur in a thermal gas-phase process.) The determined GA_{app} of each doubly-protonated peptide is listed in Table 2. Note that a numerical lower GA_{app} value means that an ion more readily donates a proton (i.e., is more acidic) and a higher value means that an ion more readily retains a proton (i.e., is more basic).

For the values of Table 2, the uncertainties listed were determined from the GB range of the two bracketing reference compounds (before and after a reaction efficiency of 0.10) and from the uncertainties associated with the reference compound GBs. The reference basicities are often reported to be known to within ±0.2 kcal/mol, although error limits are ±2 kcal/mol for some compounds. As a conservative measure, a range of 2 kcal/mol has been included in all reported uncertainties in Table 2 to account for errors associated with reference compound GBs.

SORI-CID fragmentation for the peptide ions under investigation are listed in Table 3. The peptide fragment ion nomenclature is based on that proposed by Roepstorff and Fohlman [60] and modified

Table 1
Deprotonation reaction efficiencies for $[M + 2H]^{2+}$ from bradykinin and its fragment peptides

Reference compound	GB (kcal/mol)[a]	Reaction efficiency						
		RPP	RPPG	RPPGF	RPPGFS	RPPGFSP	RPPGFSPF[b]	Bradykinin[b] RPPGFSPFR
Propylbenzene	182.2	0.01 ± 0.01[c]						
2-Butanol	187.5	0.01 ± 0.01						
Benzaldehyde	191.7	0.07 ± 0.01	0.01 ± 0.01					
Cycloheptanone	195.0	0.07 ± 0.01 BREAK[d]	0.01 ± 0.01	0.01 ± 0.01				
Acetophenone	198.3	0.20 ± 0.02	0.07 ± 0.02 BREAK	0.01 ± 0.01				
Aniline	203.3	0.13 ± 0.06	0.21 ± 0.08	0.04 ± 0.01	0.03 ± 0.01			
m-Toluidine	206.5	0.20 ± 0.12	0.26 ± 0.20	0.03 ± 0.01 BREAK	0.02 ± 0.01			
3-Fluoropyridine	208.0	0.62 ± 0.44	0.41 ± 0.03	0.20 ± 0.10	0.02 ± 0.01			
Ethylamine	210.0	0.47 ± 0.23	0.41 ± 0.02	0.18 ± 0.06	0.09 ± 0.03 BREAK	0.02 ± 0.01		
n-Propylamine	211.3	0.63 ± 0.17	0.56 ± 0.03	0.38 ± 0.07	0.26 ± 0.11	0.04 ± 0.02	0.02 ± 0.02	0.00 ± 0.00
Pyridine	214.7	0.52 ± 0.19	0.48 ± 0.03	0.33 ± 0.03	0.36 ± 0.08	0.07 ± 0.01 BREAK	0.01 ± 0.01 BREAK	0.00 ± 0.00
Cyclohexylamine	215.0	0.63 ± 0.33	0.47 ± 0.04	0.49 ± 0.12	0.41 ± 0.07	0.20 ± 0.05	0.13 ± 0.02	0.00 ± 0.00
N,*N*-Dimethylamine	217.3	0.48 ± 0.16	0.52 ± 0.04	0.42 ± 0.01	0.40 ± 0.06	0.27 ± 0.01	0.19 ± 0.06	0.00 ± 0.00
3-Methylpyridine	218.0					0.40 ± 0.03	0.16 ± 0.01	0.00 ± 0.00
Diethylamine	219.7					0.33 ± 0.04	0.33 ± 0.06	0.02 ± 0.01
Di-*i*-propylamine	224.3						0.36 ± 0.07	0.09 ± 0.04 BREAK
Triethylamine	227.3						0.33 ± 0.01	0.14 ± 0.08
Tripropylamine	229.5							0.23 ± 0.07
N,*N*,*N*′,*N*′-Tetramethyl-1,4-diaminobutane	237.3							0.30 ± 0.01

[a] All GBs of reference compounds are from [62].
[b] Results for bradykinin and des-Arg^9-bradykinin were obtained previously in our laboratory and published in [46].
[c] Reported values are mean ± S.D.
[d] BREAK indicates that the point where the GA_{app} value is assigned for the peptide ion.

Table 2
Experimental GA_{app} for $[M+2H]^{2+}$ of bradykinin and its fragment peptides

Peptide	GA_{app} (kcal/mol)
RPPGFSPFR	225.8 ± 4.2
RPPGFSPF	214.9 ± 2.3
RPPGFSP	214.9 ± 2.3
RPPGFS	210.6 ± 3.0
RPPGF	207.2 ± 3.2
RPPG	200.8 ± 5.6
RPP	196.6 ± 4.4

by Biemann [61]. The first part of Table 3 lists all N-terminal product ions, which are predominantly singly-charged b-ions. Similarly, the second part of Table 3 lists all C-terminal products, which mainly consist of the singly-charged y-series. Not present in the tables are peaks associated with water loss from the parent ion. Because all of the assigned product ions are listed in the tables, the actual CID spectra are not shown for every peptide. However, to illustrate the typical quality of the data, Fig. 1 provides the CID spectra of $[M + 2H]^{2+}$ from the octapeptide and tetrapeptide bradykinin fragments.

Coulomb and potential energy values obtained from molecular modeling for the $[M + 2H]^{2+}$ of each peptide are reported in Table 4. Protonation sites assigned for the calculations are shown in boldface. Reported Coulomb and potential energy values are averages for 25 low energy simulations involving geometry optimized structures. For each doubly-protonated peptide under study, numerous structures were found with similar potential energies within the range of a few kcal/mol. The lowest energy modeled structures proved to be good representations for the general structural trends of each doubly-protonated peptide, thus the discussion below will focus on these lowest energy structures.

3.1. *Bradykinin, Arg^1–Pro^2–Pro^3–Gly^4–Phe^5–Ser^6–Pro^7–Phe^8–Arg^9*

The GA_{app} for bradykinin $[M+2H]^{2+}$ was recently determined to be 225.8 ± 4.2 kcal/mol in our laboratory [46]. Of the peptides studied here, bradykinin ions are the most basic and least reactive by proton transfer. This is consistent with the fact that bradykinin has two arginine residues (Arg^1 and Arg^9) that are the probable protonation sites because of their very high intrinsic basicities. Arginine is by far the most basic amino acid with a GB of 240.6 kcal/mol [62,63]. In several previous studies [26,44–46], the side chains of the two terminal arginine residues have also been assumed to be the protonation sites for bradykinin $[M + 2H]^{2+}$. As we discussed in a recent publication [46], it is also possible that, under some experimental conditions, bradykinin $[M+2H]^{2+}$ may have a zwitterionic structure with two protonated arginine residues, protonation at another basic site (e.g., Pro^3 or Pro^7), and deprotonation at the C-terminal carboxylic acid group. For singly-charged bradykinin ions, numerous studies [31,34–40] using a variety of techniques suggest that a similar salt-bridge zwitterionic structure is the most stable gas-phase conformer.

The SORI-CID spectrum of the $[M + 2H]^{2+}$ for bradykinin is dominated by singly-charged b- and y-ions. Cleavage does not occur at every residue and is preferential adjacent to the proline or arginine residues. Fragmentation at the amide bond to proline is often dominant in peptide CID spectra [2,64–66]. In peptide ions containing highly basic arginine residues, it is well established that sequestering the charge on arginine side chains limits backbone dissociation [1–5]. Thus, the general lack of fragmentation in the bradykinin $[M + 2H]^{2+}$ SORI-CID spectrum is consistent with the two arginine residues being protonation sites.

The use of CID to determine protonation sites for peptides must be done with caution because protons movement is possible, especially in cases of high Coulomb repulsion between potential charge sites [5,7,8,67]. Thus, in discussions of CID products it should be kept in mind that the data can provide support for protonation sites, but not conclusive evidence. For bradykinin $[M + 2H]^{2+}$, the presence of b_1^+ and y_1^+ in the SORI-CID spectrum are consistent with protonation at the highly basic residues of Arg^1 and Arg^9, respectively. Complementary pairs of b- and y-ions may also provide information on protonation

Table 3
SORI-CID products of bradykinin and its fragment peptides

$[M + 2H]^{2+}$	b_1^+	b_2^+	$[b_2\text{-}17]^+$	$[b_2\text{-}17\text{-}18]^+$	$[b_2\text{-}58]^+$	$[b_2\text{-}17\text{-}58]^+$	b_3^+	b_4^+	b_5^+	b_6^+	$[b_6\text{-}18]^+$	$[b_6\text{-}36]^+$	b_7^+	b_8^+	$[b_8\text{-}18]^+$	Others
N-terminal CID products																
RPPGFSPFR	s	w												m	w	a_8^+(w), $[a_8\text{-}18]^+$(w)
RPPGFSPF	w	w	w		w				w	m	s	w		–	–	b_7^{2+}(m)
RPPGFSP		m							w	s	m		–	–	–	b_6^{2+}(w)
RPPGFS		s						w	s	–	–	–	–	–	–	
RPPGF	w	s	w		w			s	–	–	–	–	–	–	–	
RPPG		s	w	w				–	–	–	–	–	–	–	–	
RPP		s	w			w	–	–	–	–	–	–	–	–	–	$[a_1\text{-}17]^+$
	y_8^+	y_7^+	y_6^+	$[y_6\text{-}18]^+$	y_5^+	$[y_5\text{-}18]^+$	y_4^+	$[y_4\text{-}18]^+$	y_3^+	$[y_3\text{-}17]^+$	$[y_3\text{-}18]^+$	y_2^+	$[y_2\text{-}18]^+$	y_1^+	Others	
C-terminal products																
RPPGFSPFR	w	m	m	w					w					m	y_8^{2+}(w), z_3^+(w), $[y_8\text{-}R]^+$(w)	
RPPGFSPF	–		w						w	w		s		w	F(w), PGFS(w), PGFS-28(w)	
RPPGFSP	–	–			w	w					w	w	w	s		
RPPGFS	–	–	–	–			w	s					w		F(w), PGF(w)	
RPPGF	–	–	–	–	–	–			m					m	F(w), PG(m)	
RPPG	–	–	–	–	–	–	–	–				m			PP(w)	
RPP	–	–	–	–	–	–	–	–	–	–	–		m	s		

Product intensities are designated as w, m or s, where w is weak (<30% of the base peak), m is medium (30–60%), and s is strong (>60%). Dash indicates product ions that are not possible for the given peptide sequence.

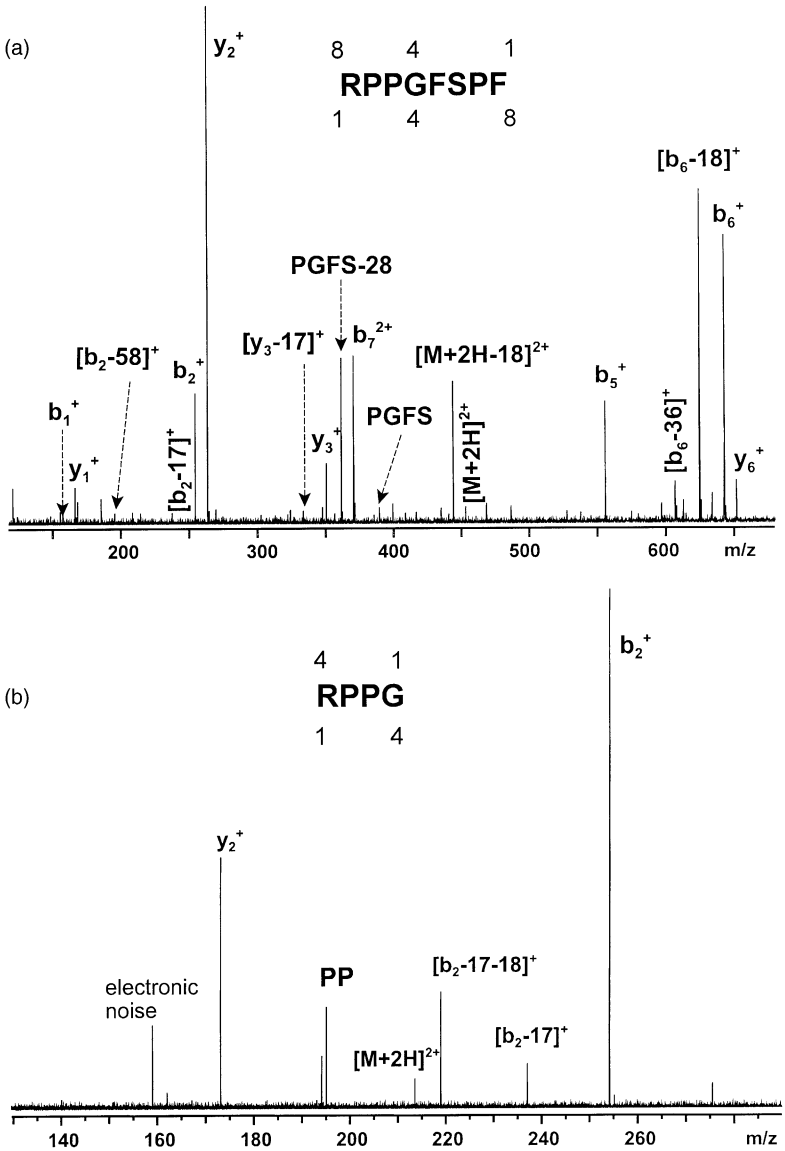

Fig. 1. SORI-CID mass spectra for $[M + 2H]^{2+}$ of (a) des-Arg^9-bradykinin and (b) the tetrapeptide Arg^1–Pro^2–Pro^3–Gly^4.

sites [2,68]. For bradykinin $[M + 2H]^{2+}$, complementary pairs of b_1^+/y_8^+, b_2^+/y_7^+, and b_8^+/y_1^+ are consistent with the proposed protonation sites.

Fig. 2 shows the lowest energy structure obtained by molecular modeling on $[M + 2H]^{2+}$ of bradykinin with the ionizing protons placed on the side chains of Arg^1 and Arg^9. The structure is very compact and has a distance between the charge sites of 6–7 Å. There are nine locations of hydrogen bonding (with lengths of 2.5 Å or less), which are shown by dashed lines in Fig. 2. Both protonated residues are heavily involved in hydrogen bonding, which should stabilize the protonation sites and contribute to the high basicity of bradykinin. Atoms on the N-terminal arginine residue,

Table 4
Molecular dynamics results for $[M + 2H]^{2+}$ from low energy structures for bradykinin and its fragment peptides

$[M + 2H]^{2+}$	Coulomb energy (kcal/mol)[a]	Potential energy (kcal/mol)[a]
RPPGFSPF**R**[b]	47 ± 14	50 ± 9
RPPGFS**P**F	44 ± 11	73 ± 9
RPPGFS**P**	46 ± 13	44 ± 5
RP**P**GFS	38 ± 5	46 ± 5
RP**P**GF	46 ± 15	29 ± 3
RP**P**G	43 ± 10	25 ± 3
RP**P**	32 ± 1	26 ± 2

[a] Mean ± S.D. for 25 modeled structures.
[b] The protonated residue for the modeling is shown in boldface.

Arg^1, participate in four hydrogen bonds to carbonyl oxygens along the peptide backbone at Pro^2, Pro^3, Ser^6, and Phe^8. The C-terminal arginine residue, Arg^9, undergoes three hydrogen bonds with its interactions involving Gly^4, Phe^5, and Pro^7. In particular, one hydrogen bond between the amide of Phe^5 and the carbonyl of Arg^1 has a length of 2.15 Å and appreciably contributes to the compactness of the structure. In addition, Pro^7 appears to be oriented in a manner that shields the protonation site of Arg^9. It is well established that proline residues have a pronounced effect on chain conformation and the process of protein folding. A proline-induced "kink" in an α-helix is often observed in globular proteins and may bend a helix by as much as 30° [69–71].

3.2. *des-Arg^9-bradykinin, Arg^1–Pro^2–Pro^3–Gly^4–Phe^5–Ser^6–Pro^7–Phe^8*

The N-terminal fragment peptides all lack bradykinin's C-terminal arginine residue. Thus, their second ionizing proton must reside at a less basic site (or sites). Intrinsic basicity considerations indicate that $[M + 2H]^{2+}$ of the fragment peptides should proton transfer more readily than ions from bradykinin itself. This was observed experimentally, with $[M + 2H]^{2+}$ from des-Arg^9-bradykinin having a GA_{app} which is 10.9 kcal/mol lower than that of bradykinin ions [46].

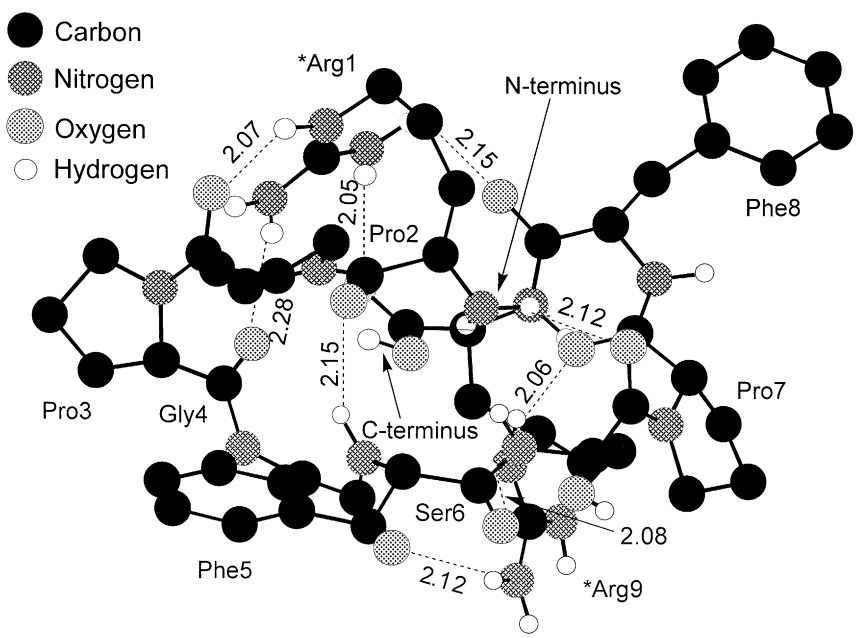

Fig. 2. Lowest energy structure for $[M + 2H]^{2+}$ of bradykinin, $^*Arg^1$–Pro^2–Pro^3–Gly^4–Phe^5–Ser^6–Pro^7–Phe^8–$^*Arg^9$. Atom legends are displayed in the top, left corner of the figure. Protonated residues are indicated with an asterisk. Hydrogen bonds are illustrated by dashed lines and the bond lengths shown are in units of angstroms.

This great difference in deprotonation energetics upon removal of Arg^9 is further evidence that both arginine residues are protonation sites in bradykinin.

For des-Arg^9-bradykinin, one protonation site is undoubtedly the side chain of Arg^1. The site (or sites) of the second proton is less clear. Protonation at the N-terminal amino group of Arg^1 is unlikely because of the high Coulomb repulsion that would result. The addition of two protons to one residue is not known to occur by ESI and, in the present study, the dipeptide Arg^1–Pro^2 did not form doubly-protonated ions. If amino acid gas-phase basicities are used as a predictor of residue basicity, the second most basic residue in these peptides is proline (GB = 214.9 kcal/mol [72]). Thus, Pro^3 or Pro^7 are potential sites of protonation. Previous molecular modeling studies by our group [46] have shown that protonation at Pro^7 lowers the energy associated with Coulombic repulsion by ca. 5 kcal/mol relative to protonation at Pro^3. However, it should be pointed out that the actual gas-phase ion population could be a mixture of two or more protonation site isomers with similar energies. Surface-induced dissociation (SID) studies by Wysocki and coworkers [7] on des-Arg^9-bradykinin $[M+2H]^{2+}$ and $[M+H]^+$ showed that the fragmentation efficiency curve for the 2+ ion was dramatically shifted to lower energy relative to the curve for the 1+ ion. This suggests that the second ionizing proton on the 2+ ion may be "mobile"; that is, not fixed to one location throughout the ion population. In addition, the amide backbones of other residues, such as Phe, may serve as protonation sites because their basicities may be similar to that of the proline backbone.

In the SORI-CID spectrum of $[M + 2H]^{2+}$ from des-Arg^9-bradykinin (see Fig. 1), the major products are y_2^+, b_2^+, b_5^+, b_6^+, and b_7^{2+}. The intense b_6^+/y_2^+ complementary pair suggests that one proton may be located somewhere on the N-terminal fragment of Arg^1–Pro^2–Pro^3–Gly^4–Phe^5–Ser^6 and another proton on the C-terminal fragment of Pro^7Phe^8. In low energy CID studies on a triple quadruple mass spectrometer, Boyd and coworkers [73] also observed this complementary pair, along with further fragmentation of b_6^+ to a_6^+. They interpreted these fragments as being consistent with protonation sites at Arg^1 and Pro^7. Only singly-charged b_6^+ formed, however, the observation of a doubly-protonated ion at b_7^{2+} provides further support for protonation of the N-terminal Arg^1 and Pro^7. The presence of b_2^+ is also consistent with protonation at or near the N-terminal residue.

Fig. 3 shows the lowest energy structure for $[M + 2H]^{2+}$ of des-Arg^9-bradykinin, with Arg^1 and Pro^7 serving as protonation sites for the modeling. The guanidino side chain of Arg^1 is surrounded by the peptide backbone. This increases hydrogen bonding and shields the protonation site. Hydrogen bonding occurs in five locations for des-Arg^9-bradykinin ions. Pro^2 and Pro^3 are involved in stabilizing the protonation site on the Arg^1 side chain through these hydrogen bonds. Hydrogen bonding between the N-terminal amino group and Pro^7 contracts the peptide structure. The other important hydrogen bond is occurring between the amide protonation site of Pro^7 and the carbonyl on Ser^6.

The modeled structures for bradykinin (Fig. 2) and des-Arg^9-bradykinin (Fig. 3) have similar general conformations. Both structures are compact with extensive hydrogen bonding. The structures have nearly identical Coulomb energies (see Table 4), which also supports conformational similarity. Consequently, changes in conformation or Coulomb energy do not account for the 10.9 kcal/mol difference in GA_{app}. This indicates that intrinsic acidity/basicity of the site being deprotonated is the dominant factor here. That is, double protonated des-Arg^9-bradykinin is significantly more reactive to proton transfer (i.e., more acidic) than doubly-protonated bradykinin because the site being deprotonated on des-Arg^9-bradykinin is of lower basicity than the highly basic Arg^9 residue of bradykinin.

3.3. *Heptapeptide, Arg^1–Pro^2–Pro^3–Gly^4–Phe^5–Ser^6–Pro^7*

The GA_{app} of $[M + 2H]^{2+}$ for the heptapeptide is 214.9 ± 2.3 kcal/mol, which is identical to the value obtained for ions of the des-Arg^9-bradykinin octapeptide. This indicates that Phe^8 does not contribute any additional stabilizing factors to the protonated ion.

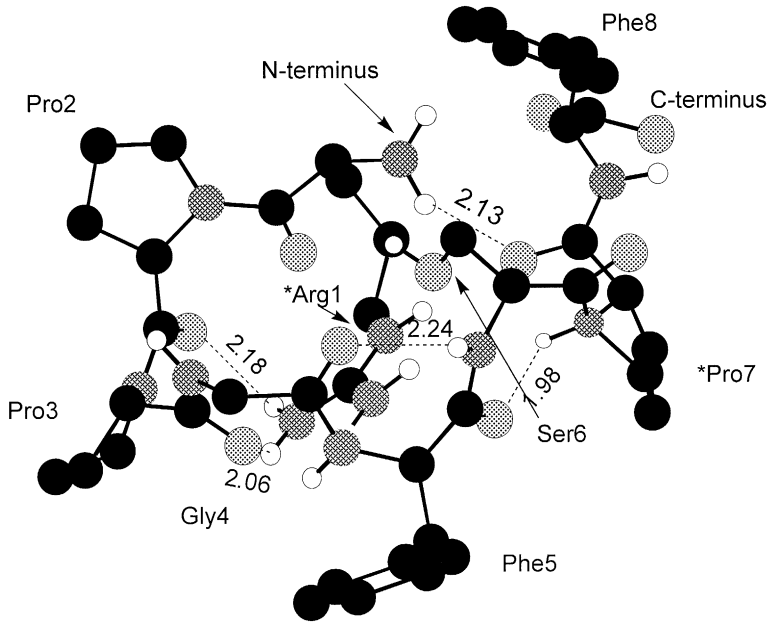

Fig. 3. Lowest energy structure for $[M + 2H]^{2+}$ of des-Arg^9-bradykinin, *Arg^1–Pro^2–Pro^3–Gly^4–Phe^5–Ser^6–*Pro^7–Phe^8. Atom legends are the same as Fig. 2. Protonated residues are indicated with an asterisk. Hydrogen bonds are illustrated by dashed lines and the bond lengths shown are in units of angstroms.

This conclusion is supported by the modeled structure of Fig. 3, which shows Phe^8 to be jutting away from the peptide backbone and uninvolved in hydrogen bonding.

The SORI-CID spectrum is once again dominated by singly-charged b- and y-ions. All possible b ions are present except for b_1^+ and b_3^+. For the y-series, y_1^+, y_2^+ and y_5^+ occur. The very intense complementary pair of y_1^+/b_6^+ supports protonation on Pro^7 and somewhere on the first six N-terminal residues. Formation of b_2^+ suggests that the Arg^1–Pro^2 region is protonated.

The lowest energy structure for the heptapeptide $[M + 2H]^{2+}$ has four hydrogen bonds, three of which involve the N-terminal protonated residue Arg^1 (Fig. 4). The highly folded nature of the peptide also leads to a hydrogen bonding interaction between Arg^1 and Pro^7, which are the two protonated residues in this model. The structure shows the amide bond of Pro^7 to be oriented towards the center of the structure, which may lessen its accessibility by the reactant base.

The calculated structures for the heptapeptide with Arg^1 and Pro^7 protonated have an average Coulomb energy of 46 ± 13 kcal/mol. Keeping the same general conformation but changing a protonation site from Pro^7 to Pro^3 increases the Coulomb energy to ca. 56 ± 7 kcal/mol. This is significantly higher than the Coulomb energies for the other ions involved in this study and suggests that protonation at Pro^7 is preferred over protonation at Pro^3.

3.4. *Hexapeptide, Arg^1–Pro^2–Pro^3–Gly^4–Phe^5–Ser^6*

The GA_{app} of $[M + 2H]^{2+}$ for the hexapeptide is 210.6 ± 3.0 kcal/mol, which is 4.3 kcal/mol less than that of the heptapeptide ions. This relatively large drop in GA_{app} is consistent with Pro^7 serving as a protonation site for at least some of the hepta- and octapeptide ion populations. ESIs ability to continue to produce the 2+ charge state once Pro^7 is removed means that the second ionizing proton can also be located

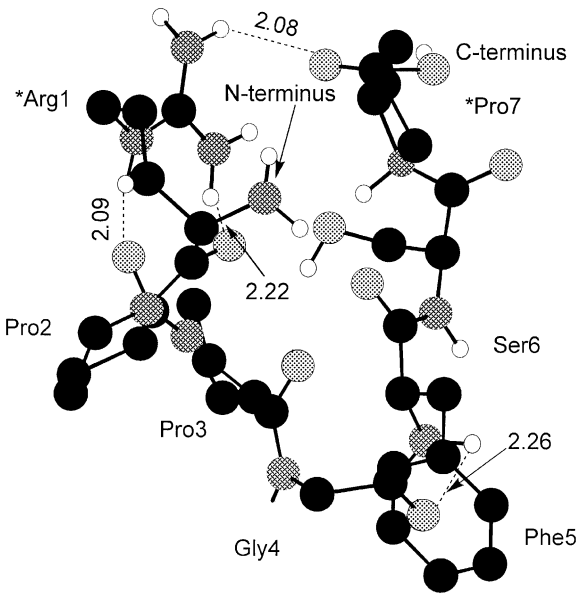

Fig. 4. Lowest energy structure for $[M+2H]^{2+}$ of the heptapeptide, $^{*}Arg^{1}$–Pro^{2}–Pro^{3}–Gly^{4}–Phe^{5}–Ser^{6}–$^{*}Pro^{7}$. Atom legends are the same as Fig. 2. Protonated residues are indicated with an asterisk. Hydrogen bonds are illustrated by dashed lines and the bond lengths shown are in units of angstroms.

at sites further down the peptide backbone. Intrinsic basicity of the remaining residues suggests that Pro^{2} or Pro^{3} is protonated, although other amide backbone sites cannot be ruled out. Minimization of Coulomb energy points to protonation at Pro^{3}, rather than Pro^{2}.

For the SORI-CID spectrum of hexapeptide $[M + 2H]^{2+}$, an intense complementary pair is seen with b_2^+ and y_4^+ or $[y_4\text{-}H_2O]^+$. The b_2^+ signifies that a proton most likely resides on Arg^{1}, as expected. The y_4^+ and associated $[y_4\text{-}H_2O]^+$ suggests that the other proton is somewhere on the Pro^{3}–Gly^{4}–Phe^{5}–Ser^{6} portion of the peptide, which supports protonation at Pro^{3}. The presence of b_4^+ and b_5^+ suggests that the second proton can be mobile during the fragmentation process and illustrates that CID data must be interpreted cautiously.

Using Arg^{1} and Pro^{3} as protonation sites, the lowest energy modeled structure has three hydrogen bonds (Fig. 5). Two hydrogen bonds at Pro^{3} and Phe^{5} are involved in stabilizing the protonated side chain of Arg^{1}. The other hydrogen bond is between the carbonyl of Arg^{1} and the protonation site on Pro^{3}. Note that as the

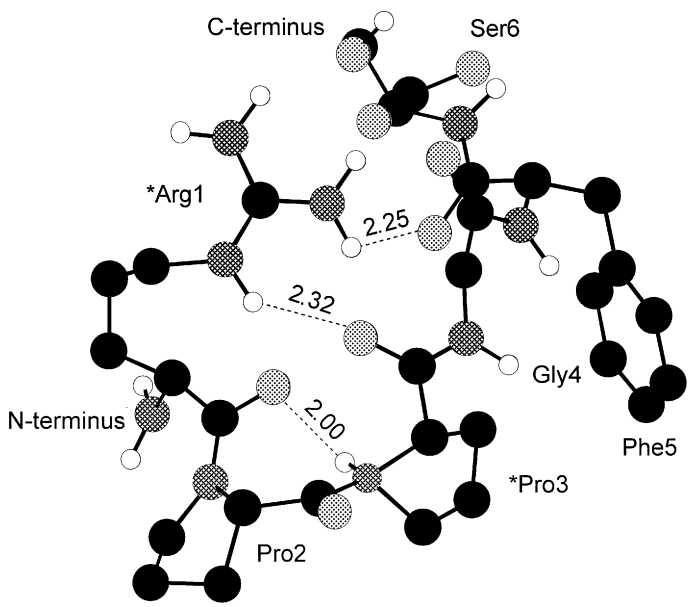

Fig. 5. Lowest energy structure for $[M + 2H]^{2+}$ of the hexapeptide, $^{*}Arg^{1}$–Pro^{2}–$^{*}Pro^{3}$–Gly^{4}–Phe^{5}–Ser^{6}. Atom legends are the same as Fig. 2. Protonated residues are indicated with an asterisk. Hydrogen bonds are illustrated by dashed lines and the bond lengths shown are in units of angstroms.

peptide chain length decreases, the number of hydrogen bonds also decrease.

The conformation of $[M+2H]^{2+}$ from the hexapeptide is less compact than that of the larger bradykinin fragments. This can be seen by comparing Fig. 5 with Figs. 2–4. (All of the modeled structures are drawn to the same scale.) Also, as seen from the data of Table 4, the average hexapeptide structure has a Coulomb energy that is 7 kcal/mol lower than that of the larger ions. This lessening of Coulomb energy means that the charges are further apart in Fig. 5. Lowering of the Coulomb energy would make the peptide less reactive to deprotonation (i.e., increases GA_{app}). However, this factor is offset by the lowered incidence of hydrogen bonding, which would make the ion more reactive (i.e., decreases GA_{app}).

3.5. *Pentapeptide, Arg^1–Pro^2–Pro^3–Gly^4–Phe^5*

The GA_{app} of $[M + 2H]^{2+}$ for the pentapeptide is 207.2 ± 3.2 kcal/mol, which is 3.4 kcal/mol less than that of the hexapeptide ions. This is a relatively small decrease in GA_{app} in comparison to the removal of other residues from the bradykinin chain. The implication is that Ser^6 plays a minimal role in interacting with the protonation sites of the hexapeptide ions. This is consistent with the modeled structure of Fig. 5, which shows Ser^6 to be jutting away from the remainder of the peptide backbone.

For SORI-CID on $[M + 2H]^{2+}$ of the pentapeptide, all b-ions form except b_3^+, which is not observed for any of the bradykinin-related peptides. For the y-series, y_1^+ and y_3^+ are present. Again, b_2^+ supports the presence of a proton near the N-terminus, while y_3^+ suggests that an ionizing proton resides on the C-terminal residues of Pro^3–Gly^4–Phe^5.

The lowest energy structure of $[M + 2H]^{2+}$ from the pentapeptide is shown in Fig. 6, with protonation sites at Arg^1 and Pro^3. The number of hydrogen bonds has decreased to two, but they significantly impact the conformation. Hydrogen bonding between Phe^5 and Pro^2 results in a more compact structure and the phenyl group of Phe^5 is oriented to enable some shielding of the protonation site on Pro^3. The orientation of Pro^2 may also shield the proton on Pro^3. Hydrogen bonding between the side chain of Arg^1 and the C-terminal carboxylate group also compacts the structure and may make the ion more basic (relative to a protonation site without hydrogen bonding).

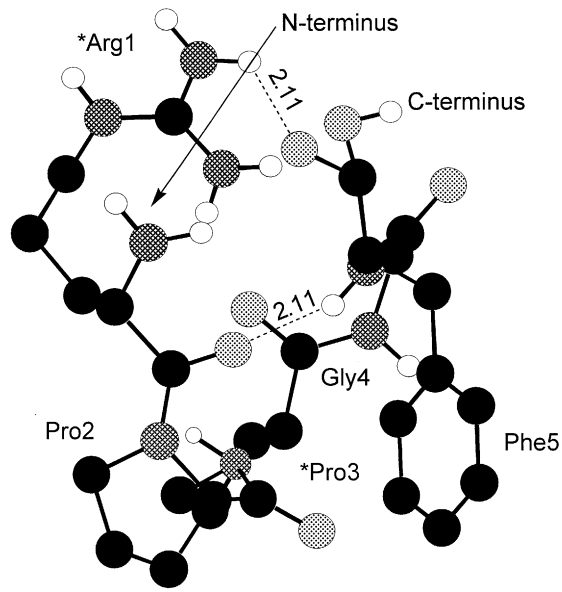

Fig. 6. Lowest energy structure for $[M + 2H]^{2+}$ of the pentapeptide, *Arg^1–Pro^2–*Pro^3–Gly^4–Phe^5. Atom legends are the same as Fig. 2. Protonated residues are indicated with an asterisk. Hydrogen bonds are illustrated by dashed lines and the bond lengths shown are in units of angstroms.

A comparison of Figs. 5 and 6 shows that the Ser^6 residue does not play a major role in the conformation. For example, in Fig. 5, no heteroatoms on Ser^6 are involved in hydrogen bonding. However, removal of Ser^6 does cause the peptide ions to contract in size slightly. As seen in Table 4, this leads to an increase in the Coulomb energy back to the levels of ions from bradykinin and the larger fragment peptides. This increased Coulomb energy may contribute to the pentapeptide ions greater proton transfer reactivity relative to the hexapeptide ions.

3.6. *Tetrapeptide, Arg^1–Pro^2–Pro^3–Gly^4*

The removal of Phe^5 to produce the tetrapeptide decreases the GA_{app} of $[M + 2H]^{2+}$ by 6.4 to

200.8 ± 5.6 kcal/mol. This large drop in energy suggests that the hydrogen bonds involving the carbonyl oxygen and the amide nitrogen of phenylalanine were involved in stabilizing protonated structure of the pentapeptide ion. It is also possible that the amide group of phenylalanine serves as a protonation site for some of the doubly-protonated pentapeptide population. In addition, as mentioned above, shielding of the protonation site at Pro^3 may also limit the pentapeptide ions' rate of proton transfer.

In the SORI-CID spectrum of $[M+2H]^{2+}$ from the tetrapeptide (see Fig. 1), the intense fragment ions of b_2^+ and y_2^+ suggest that one proton lies on Arg^1–Pro^2 and the other on Pro^3–Gly^4. The internal fragment $[Pro^2–Pro^3]^+$ further suggests that a proton is present on a proline residue. Coulomb repulsion of the two charge sites would be minimized by having Pro^3 protonated rather than Pro^2. Glycine, whose peptide side chain consists only of a hydrogen atom, is not expected to be a protonation site because it lacks a side chain heteroatom and because this residue can provide little inductive stabilization if the peptide backbone is protonated.

With Arg^1 and Pro^3 serving as protonation sites, Fig. 7 is the lowest energy structure for $[M + 2H]^{2+}$ of the tetrapeptide. The peptide backbone essentially folds in half, with hydrogen bonding between the protonation site at Arg^1 and the C-terminus at Gly^4 and between sites on Pro^2 and Pro^3. The general shapes of the lowest energy structures for tetrapeptide ions (Fig. 7) and pentapeptide ions (Fig. 6) are similar, with the phenylalanine ring of Phe^5 on the pentapeptide being uninvolved in this backbone geometry. Both structures have nearly identical Coulomb energies, which also supports conformational similarity. Consequently, major changes in conformation or Coulomb energy do not account for the 5.6 kcal/mol difference in GA_{app}. One possibility is that charge shielding the protonation site of Pro^3 by Phe^5 in the pentapeptide is the dominant factor here. That is, tetrapeptide ions are more acidic than pentapeptide ions because the protonation site at Pro^3 on the tetrapeptide is more accessible to collisions with a neutral base.

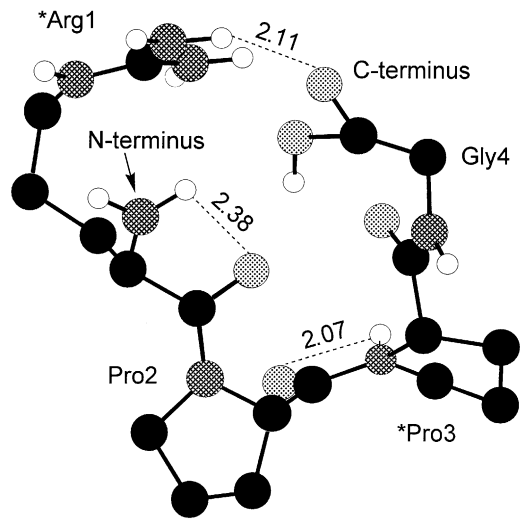

Fig. 7. Lowest energy structure for $[M+2H]^{2+}$ of the tetrapeptide, $^*Arg^1$–Pro^2–$^*Pro^3$–Gly^4. Atom legends are the same as Fig. 2. Protonated residues are indicated with an asterisk. Hydrogen bonds are illustrated by dashed lines and the bond lengths shown are in units of angstroms.

3.7. *Tripeptide, Arg^1–Pro^2–Pro^3*

The GA_{app} of $[M + 2H]^{2+}$ for the tripeptide is 196.6 ± 4.4 kcal/mol, which is a 4.2 kcal/mol drop relative to the tetrapeptide value. The tripeptide is the most acidic and most reactive of the bradykinin-related ions studied. In comparison to the hexapeptide, which is the largest ion where Arg^1 and Pro^3 are believed to be the protonation sites, the GA_{app} of tripeptide $[M + 2H]^{2+}$ is 14.0 kcal/mol lower. Thus, a substantial change in proton transfer reactivity has resulted from the loss of three residues (Gly^4–Phe^5–Ser^6) that do not sequester an ionizing proton, but can hydrogen bond to the protonation sites and sterically shield them from an incoming neutral reactant.

SORI-CID on the tripeptide ions reveals intense b_2^+ and y_1^+ product ions. This complementary pair is consistent with protonation at Arg^1 and Pro^3. In general for the peptides involved in this work, an intense b_2^+ is seen. Such enhanced fragmentation on the N-terminal side of a proline residue has also been reported in several other studies [64–66,68].

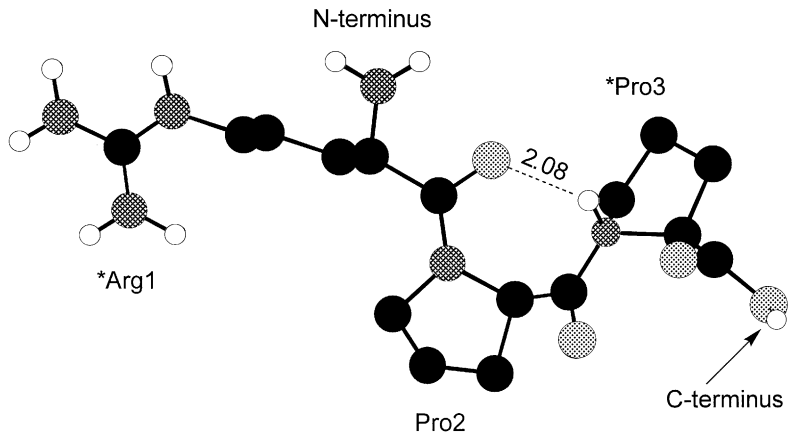

Fig. 8. Lowest energy structure for $[M + 2H]^{2+}$ of the tripeptide, $^{*}Arg^{1}–Pro^{2}–{}^{*}Pro^{3}$. Atom legends are the same as Fig. 2. Protonated residues are indicated with an asterisk. Hydrogen bonds are illustrated by dashed lines and the bond lengths shown are in units of angstroms.

The tetrapeptide and tripeptide $[M + 2H]^{2+}$ conformations are dramatically different. The tetrapeptide ion of Fig. 7 has a compact, folded structure. In contrast, the tripeptide ion of Fig. 8 is elongated. For the tripeptide, the protonated residue at Pro^{3} is slightly folded over Pro^{2}, but not to the extent observed for the larger peptides. This slight folding results in one hydrogen bond between the amide on Pro^{3} and the carbonyl of Arg^{1}. In prior work by our group, Ewing et al. [72] used semiempirical calculations on $[M + H]^{+}$ of the dipeptide ProPro to investigate its elevated basicity when compared to ions from GlyPro and ProGly. It was found that the unique geometry of proline caused the adjacent proline residues to fold towards each other, which resulted in enhanced intramolecular hydrogen bonding and lead to the high basicity of ProPro. The presence of adjacent proline residues may be a contributing factor in the ability of the small tripeptide $Arg^{1}–Pro^{2}–Pro^{3}$ to sustain two charges.

The tripeptide ion structure has a Coulomb energy that is ca. 11 kcal/mol lower than that of the larger ions. As illustrated in Fig. 8, this value corresponds to an extended conformation with the charges as far removed as possible. Lowering of Coulomb energy should decrease the rate of proton transfer. However, the overriding factors that lead to the facile deprotonation of tripeptide $[M + 2H]^{2+}$ must be the other consequences of the open conformation: decreased incidence of hydrogen bonding and greater physical accessibility of the protonation sites.

3.8. *Dipeptide, $Arg^{1}–Pro^{2}$*

The dipeptide did not produce $[M + 2H]^{2+}$ under our ESI conditions. Only $[M + H]^{+}$ was observed. This suggests that Pro^{2} was not typically protonated for the larger peptides under study here.

4. Conclusions

As residues are sequentially removed from the C-terminal side of bradykinin, a variety of factors cause the ions to more readily undergo proton transfer. The GA_{app} values for $[M + 2H]^{2+}$ decrease as the peptide chain length is shortened; this means that the ions become more acidic (i.e., less basic). The $[M + 2H]^{2+}$ of the nonapeptide bradykinin have a high GA_{app} value because its two highly basic arginine residues can serve as sequestering protonation sites. The largest decrease in GA_{app} (10.9 kcal/mol) occurs when Arg^{9} is removed from bradykinin. This can undoubtedly be attributed to the loss of a protonation site of high intrinsic basicity. Removal of the next residue, Phe^{8}, has no effect on the GA_{app} and molecular modeling shows that this residue does not

interact with the remainder of the peptide backbone. This is followed by a 4.3 kcal/mol decrease in GA_{app} upon removal of Pro^7, which is attributed to the loss of a potential protonation site at a basic proline residue. The modeled structures indicate that removal of Pro^7 also decreases the intramolecular hydrogen bonding interactions of the peptide ions, which makes the hexapeptide $[M + 2H]^{2+}$ less compact than larger bradykinin fragment peptides. In turn, this conformational change causes two opposing effects: deshielding of the protonation site (which should increase proton transfer reactivity) and lowering of the Coulomb energy (which should decrease reactivity). Removal of the next residue, Ser^6, only decreases the GA_{app} by 3.4 kcal/mol. Molecular modeling revealed that Ser^6 has little interaction with the remainder of the peptide chain. Also, this structure contains a potential protonation site, Pro^3, that is well-shielded by the peptide backbone. In contrast, a relatively large 6.4 kcal/mol decrease in GA_{app} occurs when Phe^5 is removed from the peptide structure. The loss of this bulky residue may make the protonated Pro^3 residue more accessible to the neutral reactants and also reduces the level of hydrogen bonding to Pro^3. Removal of Gly^4, to leave tripeptide ions, decreases the GA_{app} by 4.2 kcal/mol. The Arg^1 and Pro^3 residues remain on the peptide, and thus the protonation sites of the tripeptide still have the same intrinsic basicities as the protonation sites of the larger peptides. However, while the tetrapeptide ions remain relatively compact and folded, the tripeptide ions have a near linear conformation that bears little resemblance to the larger peptide ion conformations. Although nine intramolecular hydrogen bonds are seen for bradykinin ions, the number of hydrogen bonds decreases as the peptide chain length decreases until finally only one hydrogen bond remains for the tripeptide ions. When Pro^3 is removed to leave only the dipeptide $[M + 2H]^{2+}$ is no longer formed by ESI. This strongly suggests that Pro^3 is a protonation site for the larger peptides and that the adjacent residues of Arg^1 and Pro^2 cannot be simultaneously protonated under ESI conditions.

In summary, there is no single event that causes the bradykinin-related ions to deprotonate more readily as the peptide chain length decreases. Depending upon the situation, factors that can play a role in proton transfer reactivity include intrinsic basicity of the protonation sites, intramolecular hydrogen bonding (particularly involving the protonated residue), Coulombic repulsion of charge sites, and conformational considerations such as accessibility or shielding of the protonation site.

Acknowledgements

Financial support from the National Institutes of Health (R01-GM51384) is gratefully acknowledged. Much of this work was performed while the authors were employed at the Department of Chemistry and Biochemistry, Miami University, Oxford, OH 45056.

References

[1] R.W. Vachet, M.R. Asam, G.L. Glish, J. Am. Chem. Soc. 118 (1996) 6252.
[2] X.J. Tang, P. Thibault, R.K. Boyd, Anal. Chem. 65 (1993) 2824.
[3] R.S. Johnson, S.A. Martin, K. Biemann, Int. J. Mass Spectrom. Ion Proc. 86 (1988) 137.
[4] S.A. Martin, K. Biemann, Int. J. Mass Spectrom. Ion Proc. 78 (1987) 213.
[5] S.G. Summerfield, S.J. Gaskell, Int. J. Mass Spectrom. Ion Proc. 165 (1997) 509.
[6] K.M. Downard, K. Biemann, J. Am. Soc. Mass Spectrom. 5 (1994) 966.
[7] A.R. Dongre, J.L. Jones, A. Somogyi, V.H. Wysocki, J. Am. Chem. Soc. 118 (1996) 8365.
[8] X. Zhang, J. Jai-nhuknan, C.J. Cassady, Int. J. Mass Spectrom. Ion Proc. 171 (1997) 135.
[9] S. Petrie, G. Javahery, D.K. Bohme, Int. J. Mass Spectrom. Ion Proc. 124 (1993) 145.
[10] S. Petrie, G. Javahery, H. Wincel, D.K. Bohme, J. Am. Chem. Soc. 115 (1993) 6290.
[11] E.R. Williams, J. Mass Spectrom. 31 (1996) 831.
[12] C.J. Cassady, in: A. Greenberg, C.M. Breneman, J.F. Liebman (Eds.), The Amide Linkage: Structural Significance in Chemistry, Biochemistry, and Materials Science, Wiley-Interscience, London, 2000, Gas-Phase Ion Chemistry of Amides, Peptides, and Proteins, p. 463.
[13] M.K. Green, C.B. Lebrilla, Mass Spectrom. Rev. 16 (1997) 53.
[14] S.R. Carr, C.J. Cassady, J. Mass Spectrom. 32 (1997) 959.
[15] X. Zhang, C.J. Cassady, J. Am. Soc. Mass Spectrom. 7 (1996) 1211.

[16] X. Zhang, N.P. Ewing, C.J. Cassady, Int. J. Mass Spectrom. Ion Proc. 175 (1998) 159.
[17] C.J. Cassady, J. Am. Soc. Mass Spectrom. 9 (1998) 716.
[18] S.A. McLuckey, G.J. Van Berkel, G.L. Glish, J. Am. Chem. Soc. 112 (1990) 5668.
[19] R. Houriet, H. Rufenacht, P.-A. Carrupt, P. Vogel, M. Tichy, J. Am. Chem. Soc. 105 (1983) 3417.
[20] D.S. Gross, P.D. Schnier, S.E. Rodriguez-Cruz, C.K. Fagerquist, E.R. Williams, Proc. Natl. Acad. Sci. U.S.A. 93 (1996) 3143.
[21] R.R. Ogorzalek Loo, B.E. Winger, R.D. Smith, J. Am. Soc. Mass Spectrom. 5 (1994) 1064.
[22] J. Wang, C.J. Cassady, Int. J. Mass Spectrom. 182/183 (1999) 233.
[23] S.J. Valentine, J.G. Anderson, A.D. Ellington, D.E. Clemmer, J. Phys. Chem. 101 (1997) 3891.
[24] A.C. Gill, K.R. Jennings, T. Wyttenbach, M.T. Bowers, Int. J. Mass Spectrom. 195/196 (2000) 685.
[25] T.G. Schaaff, J.L. Stephenson, S.A. McLuckey, J. Am. Chem. Soc. 121 (1999) 8907.
[26] T.G. Schaaff, J.L. Stephenson, S.A. McLuckey, J. Am. Soc. Mass Spectrom. 11 (2000) 167.
[27] P.D. Schnier, J.C. Jurchen, E.R. Williams, J. Phys. Chem. B 103 (1999) 737.
[28] S.C. Henderson, S.J. Valentine, A.E. Counterman, D.E. Clemmer, Anal. Chem. 71 (1999) 291.
[29] I.D. Figueroa, D.H. Russell, J. Am. Soc. Mass Spectrom. 10 (1999) 719.
[30] D.J. Butcher, K.G. Asano, D.E. Goeringer, S.A. McLuckey, J. Phys. Chem. A 103 (1999) 8664.
[31] M.A. Freitas, A.G. Marshall, Int. J. Mass Spectrom. 182/183 (1999) 221.
[32] T. Wyttenbach, G. von Helden, M.T. Bowers, J. Am. Chem. Soc. 118 (1996) 8355.
[33] G.C. Thorne, K.D. Ballard, S.J. Gaskell, J. Am. Soc. Mass Spectrom. 1 (1990) 249.
[34] M.J. Deery, S.G. Summerfield, A. Buzy, K. Jennings, J. Am. Soc. Mass Spectrom. 8 (1997) 253.
[35] W.D. Price, R.A. Jockusch, E.R. Williams, J. Am. Chem. Soc. 119 (1997) 11988.
[36] P.D. Schnier, W.D. Price, R.A. Jockusch, E.R. Williams, J. Am. Chem. Soc. 118 (1996) 7178.
[37] S.W. Lee, H.S. Kim, J.L. Beauchamp, J. Am. Chem. Soc. 120 (1998) 3188.
[38] S.G. Summerfield, A. Whiting, S.J. Gaskell, Int. J. Mass Spectrom. Ion Proc. 162 (1997) 149.
[39] K.A. Cox, S.J. Gaskell, M. Morris, A. Whiting, J. Am. Soc. Mass Spectrom. 7 (1996) 522.
[40] E.F. Strittmatter, E.R. Williams, J. Phys. Chem. A 104 (2000) 6069.
[41] T. Wyttenbach, M.T. Bowers, J. Am. Soc. Mass Spectrom. 10 (1999) 9.
[42] S. Fang, T. Takao, Y. Satomi, W. Mo, Y. Shimonishi, J. Am. Soc. Mass Spectrom. 11 (2000) 345.
[43] M.E. Gimon-Kinsel, D.C. Barbacci, D.H. Russell, J. Mass Spectrom. 34 (1999) 124.
[44] W.D. Price, P.D. Schnier, E.R. Williams, Anal. Chem. 68 (1996) 859.
[45] Z. Szilagyi, L. Drahos, K. Vekey, J. Mass Spectrom. 32 (1997) 689.
[46] N.P. Ewing, G.A. Pallante, X. Zhang, C.J. Cassady, J. Mass Spectrom. 36 (2001) 875.
[47] A.J.R. Heck, L.J. de Koning, F.A. Pinkse, N.M.M. Nibbering, Rapid Commun. Mass Spectrom. 5 (1991) 406.
[48] J.E. Bartmess, R.M. Georgiadis, Vacuum 33 (1983) 149.
[49] J.E. Bartmess, in: P. Ausloos, S.G. Lias (Eds.), Structure/Reactivity and Thermochemistry of Ions, Reidel, Dordrecht, The Netherlands, 1987, Ion Thermochemistry: Summary of the Panel Discussion, p. 367.
[50] T. Su, W.J. Chesnavich, J. Chem. Phys. 76 (1982) 5183.
[51] T. Su, J. Chem. Phys. 89 (1988) 5355.
[52] J.W. Gauthier, T.R. Trautman, D.B. Jacobson, Anal. Chim. Acta 246 (1991) 211.
[53] A. Greenberg, in: A. Greenberg, C.M. Breneman, J.F. Liebman (Eds.), The Amide Linkage: Structural Significance in Chemistry, Biochemistry, and Materials Science, Wiley-Interscience, New York, 2000, The Amide Linkage as a Ligand: Its Properties and the Role of Distortion, p. 47.
[54] P.D. Schnier, D.S. Gross, E.R. Williams, J. Am. Soc. Mass Spectrom. 6 (1995) 1086.
[55] B.R. Brooks, R.E. Bruccoleri, B.D. Olafson, D.J. States, S. Swaminathan, M. Karplus, J. Comput. Chem. 4 (1983) 187.
[56] D.S. Gross, S.E. Rodriguez-Cruz, S. Bock, E.R. Williams, J. Phys. Chem. 99 (1995) 4034.
[57] D.S. Gross, E.R. Williams, J. Am. Chem. Soc. 117 (1995) 883.
[58] S. Gronert, J. Am. Chem. Soc. 118 (1996) 3525.
[59] E. Gard, M.K. Green, J. Bregar, C.B. Lebrilla, J. Am. Soc. Mass Spectrom. 5 (1994) 623.
[60] P. Roepstorff, J. Fohlman, Biomed. Mass Spectrom. 11 (1984) 601.
[61] K. Biemann, Biomed. Environ. Mass Spectrom. 16 (1988) 99.
[62] E.P. Hunter, S.G. Lias, in: W.G. Mallard, P.J. Linstrom (Eds.), NIST Chemistry WebBook, NIST Standard Reference Database Number 69, National Institute of Standards and Technology, Gaithersburg, MD, February 2000, Proton Affinity Evaluation (http://webbook.nist.gov).
[63] Z. Wu, C. Fenselau, Rapid Commun. Mass Spectrom. 6 (1992) 403.
[64] T. Vaisar, J. Urban, J. Mass Spectrom. 31 (1996) 1185.
[65] J.A. Loo, C.G. Edmonds, R.D. Smith, Anal. Chem. 65 (1993) 425.
[66] B.L. Schwartz, M.M. Bursey, Biol. Mass Spectrom. 21 (1992) 92.
[67] R.S. Johnson, D. Krylov, K.A. Walsh, J. Mass Spectrom. 30 (1995) 386.
[68] C.J. Cassady, S.R. Carr, J. Mass Spectrom. 31 (1996) 247.
[69] K.A. Williams, C.M. Beber, Biochemistry 30 (1991) 8919.
[70] G. Vanhoof, F. Goosens, I. De Meester, D. Hendriks, S. Scharpe, FASEB J. 9 (1995) 736.
[71] D.J. Barlow, J.M. Thornton, J. Mol. Biol. 201 (1988) 601.
[72] N.P. Ewing, X. Zhang, C.J. Cassady, J. Mass Spectrom. 31 (1996) 1345.
[73] X. Tang, P. Thibault, R.K. Boyd, Anal. Chem. 65 (1993) 2824.